Analysis of blue corona discharges at the top of tropical thunderstorm clouds in different phases of convection

Krystallia Dimitriadou[1], Olivier Chanrion[2], Torsten Neubert[3], Alain Protat[4], Valentin Louf[5], Matthias Heumesser[2], Lasse Husbjerg[1], Christoph Köhn[6], Nikolai Østgaard[7], and Víctor Reglero[8]

[1]National Space Institute, Technical University of Denmark (DTU Space)
[2]National Space Institute (DTU Space)
[3]Department of Solar System Physics, Denmark
[4]Australian Bureau of Meteorology
[5]Monash University
[6]Technical University of Denmark
[7]Birkeland Centre for Space Science,University of Bergen
[8]University of Valencia

November 22, 2022

Abstract

We report on observations of corona discharges at the uppermost region of clouds characterized by emissions in a blue band of nitrogen molecules at 337 nm, with little activity in a red band of lightning leaders at 777.4 nm. Past work suggests they are generated in cloud tops reaching the tropopause and above. Here we explore their occurrence in two convection environments of the same storm: one is developing with clouds reaching above the tropopause, and one is collapsing with lower clouds. We focus on those that form a distinct category with fast risetimes below 20 µs, signifying they are at the very top of the clouds. The discharges are observed in both environments. In the collapsing cells they are related to substructures of convection. The observations suggest that a range of storm environments may generate corona discharges, and that they may be quite common in convective surges.

1

Analysis of blue corona discharges at the top of tropical thunderstorm clouds in different phases of convection

Krystallia Dimitriadou[1], Olivier Chanrion[1], Torsten Neubert[1], Alain Protat[2], Valentin Louf[2], Matthias Heumesser[1], Lasse Husbjerg[1], Christoph Köhn[1], Nikolai Østgaard[3], and Victor Reglero[4]

[1]National Space Institute, Technical University of Denmark (DTU Space), Kgs. Lyngby, Denmark

[2]Australian Bureau of Meteorology, Science and Innovation Group, Radar Science and Nowcasting Team, Melbourne, Australia

[3]University of Bergen, Birkeland Centre for Space Science, Bergen, Norway

[4]University of Valencia, Image Processing Laboratory, Valencia, Spain

Key Points:

- Corona discharges at cloud tops form a distinct type of electric discharges with rise times <20 μs in 337 nm and little activity in 777.4 nm
- They are generated both in developing storm cells overshooting the tropopause height and collapsing cells close to convective activity
- Some are detected by ground-based sensors often with negative polarity implying they are fast break-down discharges with high current pulses

---

Corresponding author: Krystallia Dimitriadou, `krstd@space.dtu.dk`

Abstract

We report on observations of corona discharges at the uppermost region of clouds characterized by emissions in a blue band of nitrogen molecules at 337 nm, with little activity in a red band of lightning leaders at 777.4 nm. Past work suggests they are generated in cloud tops reaching the tropopause and above. Here we explore their occurrence in two convection environments of the same storm: one is developing with clouds reaching above the tropopause, and one is collapsing with lower clouds. We focus on those that form a distinct category with fast risetimes below 20 µs, signifying they are at the very top of the clouds. The discharges are observed in both environments. In the collapsing cells they are related to substructures of convection. The observations suggest that a range of storm environments may generate corona discharges, and that they may be quite common in convective surges.

Plain Language Summary

Discharges in thunderstorm clouds that have no or little lightning leader emissions are from cold streamers and are called corona discharges. They are thought to be generated in the upper regions of high clouds that may reach into the stratosphere. Here we explore if storms with lower cloud tops also may generate these, by comparing measurements of a collapsing and a developing thunderstorm environment that both are part of a larger storm system. We find that the discharges are created in both environments. In the collapsing system they appear associated with substructures of convection. The results show that a range of thunderstorm environments may generate blue corona discharges and that they therefore may be quite common.

1 Introduction

Blue electrical discharges may form in the top of thunderstorm clouds and propagate upwards to altitudes as high as the stratopause at 50 km and even the ionosphere at ∼80 km. They include the gigantic jets, blue jets, blue starters, pixies, gnomes and km-scale corona discharges (Wescott et al., 1995; Lyons et al., 2003; Krehbiel et al., 2008; Chou et al., 2010; N. Liu et al., 2015; Chanrion et al., 2017). They represent a coupling between the troposphere and the stratosphere powered by the underlying convective activity of the parent thunderstorms. Unlike optical emissions in the mesosphere, such as sprites and elves, they are difficult to detect from the ground because the clouds obstruct their view. Therefore, studies are often based on observations from space that allow for an unimpeded view of the discharges (Kuo et al., 2009; Chou et al., 2010; N. Liu et al., 2015; Chanrion et al., 2017; Neubert et al., 2021).

The most prominent meteorological environments for the production of blue discharges are moist tropical or tropical-like thunderstorms (Meyer et al., 2013; N. Liu et al., 2015; Lazarus et al., 2015; Chanrion et al., 2017; Boggs et al., 2018) either multi-cellular in their formation (Wescott et al., 1995; Edens, 2011; Suzuki et al., 2012), super-cell type (van der Velde et al., 2007), or in isolated cells (Chou et al., 2010; Neubert et al., 2021) or shallow winter thunderstorms (Van Der Velde et al., 2010). They tend to originate near overshooting tops of convective clouds during the developing/mature stage of a storm. However, observations are scarce. We have therefore analyzed optical and UV-measurements by the Atmospheres-Space Interactions Monitor (ASIM) as it passed over a thunderstorm in the region of Darwin, Australia, during the southern hemisphere summer. The storm is interesting because it includes a convective region with high clouds and a dissipating region with lower clouds.

Blue corona discharges in clouds are of a few tens of microsecond duration and are characterized by the absence of lightning leader emissions, commonly measured in a narrow band around the atomic oxygen line at 777.4 nm (Christian et al., 1989). They are therefore emissions from cold streamers, sometimes referred to as streamer coronae (Soler et al., 2020).

Corona emissions observed from space may appear with a range of rise times that reflect the amount of photon scattering by the cloud particles. The rise time, therefore, is a measure of the depth in clouds of the discharges. The polarity of the discharges depends on the polarity of the charge layers where they originate. Discharges some kilometres below the cloud tops have been related to positive polarity narrow bipolar events (NBEs), which are signatures in electromagnetic waveform data in the frequency range 3-300 MHz that have a brief duration of 10-30 µs (Wu et al., 2012; Soler et al., 2020). Blue discharges at the cloud tops have been associated with negative NBEs (F. Liu et al., 2018; Chou et al., 2018; F. Liu et al., 2021), generated in the regions of the upper positive charge layer and the negative screening layer above. They may mark the onset of lightning (Tilles et al., 2019) and of blue jets to the stratosphere (Neubert et al., 2021).

The analysis we present in this paper is focused on the cloud-top discharges with fast rise times. We first present the methodology and data sources of the study, then the observations and analysis, and finally a discussion.

2 Data Sources and Methods

The blue discharges are observed by ASIM on the International Space Station (ISS), a suite of nadir-pointing instruments for measurements of conventional lightning, Transient Luminous Events (TLEs) and Terrestrial Gamma-ray Flashes (TGFs) (Neubert et al., 2019). It includes three photometers measuring at 337.0/4 nm (blue), at 180-230 nm (UV) and at 777.4/5 nm (red), with temporal resolution of 100 kHz. It also includes two cameras in 337.0/5 nm and 777.4/3 nm running at up to 12 frames per second and a spatial resolution on the ground of 400-500 m. The blue band is associated with $N_2 2P$, one of the strongest emissions in streamer discharges. The UV band includes part of the Lyman-Birge-Hopfield system of N_2 and is particularly sensitive to high-altitude emissions such as sprites and elves. The red band selects a main emission line of lightning leaders emitted by atomic oxygen. If more than two instruments trigger on a flash, the data of all sensors are saved for downlink. An instrument event refers to a data sequence of at most 8 consecutive frames of ∼83.3 ms duration each (Chanrion et al., 2019).

As ASIM passed over the storm, a multitude of emissions were observed where the signal in the blue band dominated. A sub-group that stands out is events at the cloud top, which are seen in the ASIM data with very fast rise times (below 20 µs) that signifies the emissions are quasi unaffected by scattering in cloud particles. These events will be the focus of our analysis where we characterize the thunderstorm environment and the convection that are associated with the discharges. We then define a fast, blue discharge as one where the rise time of the blue pulse is less than 20 µs and the peak amplitude of the accompanying red pulse is less than 0.15 the peak of the blue pulse (see Supporting information for details). The source of blue emissions are thought to originate from optical depths of less than 1 km below the cloud top.

Lightning data from the GLD360 network (Said et al., 2013) and the ENTLN network (Marchand et al., 2019) are used to characterize the electric activity of the thunderstorm regions reaching from before to after the ASIM overpass, and to correlate lightning detections with blue discharges. In addition, the absolute timing of the ASIM data was corrected to an accuracy of ∼1 ms by aligning the time of the onsets of the pulses in the red photometer with the GLD360 stroke times, using the strongest pulses of 134 mutual events. Here we have neglected the propagation delay of photons from the lightning source to the detector. However, the important aspect is the correct correspondence of optical pulses measured by ASIM with lightning sources detected by ground-based networks.

The location of the blue discharges is obtained by projection to 16 km altitude, which is taken as a reference altitude of the cloud tops. The accuracy of the projection depends primarily on the accuracy of the ISS location and attitude, and the mounting of the sensors

on the ISS and is estimated to ∼20 km. Uncertainties of the GLD refer to a location accuracy median of 1.8 km and a 90th percentile location error of 6.4 km (Said & Murphy, 2016).

The meteorological context of the storm is analysed with data from the Himawari-8 geostationary satellite, supplied by the Japan Aerospace Exploration Agency (JAXA) (Bessho et al., 2016). Himawari provides the brightness temperature (BT) every 10 minutes with a spatial resolution of 2 km. The cloud top temperature (CTT) and the cloud top height (CTH) are estimated by translating the BT to CTT and then to CTH using atmospheric sounding data provided by the University of Wyoming. The closest temperature profile was taken from station 94120 YPDN at Darwin Airport (-12.42°, 130.89°). The structure and vertical extend of the storm are derived from reflectivity data from a single-polarization Doppler C-band weather radar in Berrimah, Northern Australia (-12.46°, 130.93°). It gives a full 3D volumetric scan every 6 minutes using 13 elevation angles (0.5° to 32°). These volumetric observations are then gridded at a resolution of 1 km horizontally and 500 m vertically. The radar makes 3D volumetric scans up to 150 km range, and an additional quasi-horizontal "surveillance" scan up to a 250 km range.

3 Observations and Analysis

The north-western part of Australia is characterized by frequent thunderstorms with heavy rainfall and intense lightning, especially over land (Laroche, 2009). ASIM passed over a storm in the region on January 30, 2019, between 17:02:12.519 and 17:03:43.695 UTC. Infrared satellite measurements identified two large groups of cells, a northern one with lower cloud tops (above -13.1° latitude) and a southern one with high cloud tops. They are shown in Figure 1 at 17:00 UTC. The storm began to form the day before and developed into a tropical multi-cellular thunderstorm as it moved towards the East. The atmospheric sounding (Figure S1) closest in space and time was at 12:00 UTC, and reported very humid conditions with nearly saturated air between the cloud base (∼500 m) and the tropopause (∼17.05 km) as well as extreme instability with a Convective Available Potential Energy (CAPE) of 4000 J kg^{-1}. The equilibrium level was at 17.15 km, meaning that an ascending air parcel had the potential to continue moving upwards above the tropopause layer. At the time of the overpass, the northern cells were dissipating and the southern cells were growing (Figure S2). The electrical activity of the two cells, traced by GLD360, was decreasing in the dissipating cells and increasing in the growing cells (Figures S3-4). There was a substantial wind shear with strong winds from the west and south below 7.5 km and strong winds from the east further above. This wind profile strengthens the storm since it displaces the updraft from the downdraft, thus allowing updraft motions to be sustained for longer time. A large increase in wind speed was found between 13.7 km (∼163 hPa) and the tropopause (∼91 hPa), going from ∼18 knots (∼9 m/s) at 13.7 km to ∼70 knots (∼36 m/s) at 17.05 km.

A total of 134 instrument events were observed during the overpass. They include sequences of photometer pulses from conventional lightning where both red and blue signals have significant amplitudes, and a multitude of primarily blue pulses with varying rise times. 14 pulses satisfy the criteria of fast blue discharges. For one pulse, two spots of blue activity appear in the corresponding camera frame; they are both shown in Figure 1. We see that events are detected in both regions close to the highest clouds, with most events in the developing region of the highest clouds. The distribution with rise time of all events is shown in Figure S5.

An example of a blue event is shown in Figure 2. In Figure 2a are the three photometer signals during the time of one camera frame. We see that the blue photometer signal dominates over the red. It has a peak in the middle of the frame that is almost two orders of magnitude larger than the red signal and fades during the remaining ∼40 ms of the frame. The red signal also peaks but to a smaller amplitude and is delayed by ∼1 ms. Figure 2b is a zoom on the event and is on a linear scale to illustrate the fast rise time of the blue

flash. The corresponding camera images are at the bottom panels with the blue camera image on the left (c) and the red on the right (d). The red emissions in the lower corner of the image have a correspondence with weak emissions in the blue image, whereas the blue image includes distinct emission in the upper corner, not found in the red. The photometer signals then represent two events. We identify the one in the lower corner as a lightning event at some depth in the cloud associated with the red photometer signal and the blue event in the upper corner with the blue flash. The blue flash is in frame 3 of an 8-frame sequence of pulses that primarily are blue (Figure S6).

The decay over ∼40 ms of the blue flash suggests that the discharge may rise above the cloud, as concluded for a similar event in Neubert et al. (2021). In this case we would expect to see emissions reflected in the cloud and therefore a diffuse region of the cloud surrounding the discharge. This appears to be borne out by the camera image where the blue spot (upper corner) is consistent with a diffuse region of ∼10 km diameter. A negative stroke of -9 kA, identified by the GLD sensors, appears to be correlated with pre-activity preceding the blue discharge. The differences in time and location are ∼0.7 ms and ∼10 km, which are within the accuracy of the data. It suggests that the blue flash carries a current pulse of a magnitude comparable to lightning currents with a polarity consistent with negative NBEs. Moving upwards, the discharge carries positive charge aloft.

A second example of a blue discharge is shown in Figure 3. The signal in the blue band increases two orders of magnitude within ∼20 μs and fades over the following 15-30 ms. A zoom on the event (b) shows that the UV signal reaches the amplitude of the blue signal ∼200 μs after the peak. The event is almost identical to one discussed in Neubert et al. (2021), where the UV signal was interpreted as a signature of an elve. The presence of an elve and the absence of significant red emissions suggest that significant peak currents are carried by the blue flash. This is supported by GLD360 observations of a stroke coincident in time and location (within 9.5 km) with a peak current of +102 kA. However, the polarity is positive whereas elves usually are generated by negative flashes. If the event is related to NBEs, it further suggests a positive polarity, which usually are found lower in the clouds. The camera images (c,d) show two regions with activity in both images and one exclusively in the blue. The blue region is saturated, seen as an extension of signal along the direction of a pixel row. The event is in frame 4 of an 8-frame sequence (Figure S7) that contains both blue- and red-dominated pulses. We identify the blue flash of the photometer with the blue flash of the camera. However, also in this case, the blue flash is part of a larger sequence of activity that is quite complex. There are two minor GLD strokes at +14 and +8 kA that correlate with a red peak within ∼1-2 ms, ∼9.7 km. The correlated strokes are shown on Figures 3c and 3d.

The discharge in Figure 2 is from the dissipating cloud region (northern) and the discharge in Figure 3 is from the developing region (southern). Their relation to the vertically integrated radar reflectivity is shown in Figure 4a. The integrated reflectivity is the sum of all reflectivities in a column and provides information for the ice part (convective cores) of a reflectivity profile. It also accentuates columns where the reflectivity is strong, meaning that convective cores are better identified. The 3 discharges in the northern cells are from regions of high reflectivity and cloud tops at ∼15-17 km (Figure 1) and the 12 in the southern cells are from regions of moderate to high reflectivity and cloud tops that likely reach above the tropopause, as determined by the reference radiosonde. The northern region is within a range that allows 3D vertical cross sections of the cloud. Figures 4c and 4d are scans along the latitude and longitude of the blue flash in Figure 2. The blue event falls in an unambiguous area where an overshooting top exists.

Of the 14 fast, blue events detected by the photometers, 12 correlate with strokes of negative polarity and 2 with positive polarity. Events associated with peak amplitudes above 32 kA have a small rise in the UV signal simultaneous to the blue signal with UV/blue amplitude ∼10-4. The ratio is consistent with photons from the LBH band, generated by the discharge at the cloud tops, leaking through the absorbing atmosphere to the detec-

tor (Neubert et al., 2021). There are 10 events in this category, 4 of which have additional UV pulses, as the example in Figure 3, suggesting they generate elves. These events are associated with the highest currents detected by GLD360 (>75 kA), the two strokes with positive polarity and two with negative polarity. An overview table with the properties associated with the events is shown in the Supporting Information, Table S1.

4 Discussion and Interpretation

ASIM detected 14 blue pulses with rise times below 20 μs and with an associated ratio of red/blue signal of less than 0.15. The fast rise time indicates that photons are relatively unaffected by scattering in the cloud and therefore they are at the top of the clouds. The absence of (or weak) emissions in the red (777.4 nm) indicates that no or little leader activity is associated and that the emissions are therefore of the streamer type.

The collapsing cells has 3 events and the growing cells has 12 events, both close to the regions with the highest clouds. Wiens et al. (2008) demonstrated that reflectivity can be used as a proxy for convection strength and values above 40 dBZ can indicate convective activity. In their study, they use the composite reflectivity, which is the strongest radar echo intensity from any elevation angle and reveals the highest reflectivity in all echoes. In our analysis, we use the integrated reflectivity, a sum of all reflectivities in an atmospheric column, as a more detailed measure for convection strength. The integrated reflectivity for all blue events has values of ∼25-50 dB km (Table S1). The cells can be rather small as in the case of the northern, dissipating region (Figure 1), with diameters around the accuracy of the ground projection of the ASIM events (∼20 km), and thus there is some uncertainty on the values of the integrated reflectivity and cloud top altitude associated with an event. An added complexity is that the southern region is at a relatively large distance from the radar, which may underestimate the derived integrated reflectivities. In general, higher reflectivities are indicative of larger precipitation particles, and the reflectivity cores observed in the radar cross sections (Figures 4b and 4c) extend upward because hydrometeors are being carried upwards by the intense updrafts. Lower reflectivities can have a lateral extend beyond the core and these regions can be highly electrified (Stolzenburg et al., 1998). Our observations support that the developing regions of deep convection with high clouds may generate blue corona discharges, but that these are also generated in convective substructures of dissipating regions as also suggested in Meyer et al. (2013).

The updraft motion of air in clouds facilitates the formation and growth of mixed-phase hydrometeors such as ice crystals, graupel and supercooled droplets. Collisions between these hydrometeors result in electrification processes within the cloud. Clouds need to contain precipitation size ice particles required for electrification processes. Zipser E.J. & Lutz K.R. (1994) indicated that lightning producing clouds display reflectivities greater than 30 dBZ above the freezing level, are indicative of the presence of ice. Wu et al. (2012) used this criterion and found that NBEs rates increase with the maximum altitude of ≥ 30 dBZ. In the storm we present here, the freezing level is around 4.7 km altitude, and the altitude of 30 dBZ is 5-6.5 km in the region of the three blue discharges (Figures 4b, 4c, S8, S9). We conjecture then, that although the flash rates (Figures S3 and S4) indicated dissipation of convective activity in the southern group of cells, there were enough ice hydrometeors and convection in the sub-cells to facilitate the conditions for the creation of NBEs, and thereby blue corona discharges.

Blue corona discharges, as those presented here, appear to be the equivalent of negative NBEs (F. Liu et al., 2021). Our analysis is for the most part consistent with this view. For instance, all but two discharges are associated with negative peak currents detected by ground-based lightning detection networks, and, like NBEs, the fast rise time suggests a fast streamer discharge as proposed by others for NBEs (Rison et al., 2016). We find that they are generated at cloud tops where also negative NBEs are found (Wu et al., 2013),

and are associated with regions of strong convection and high clouds (Jacobson & Heavner, 2005; Wu et al., 2012; Wiens et al., 2008; Karunarathna et al., 2015).

Thunderstorm clouds are generally assumed to have an upper positive charge region shielded by a negative charge layer above. Blue corona discharges at the cloud tops, as discussed here, and blue jets are thought to be discharges between the upper positive layer and the screening layer, whereas if the screening layers is weak or absent, gigantic jets may form (Krehbiel et al., 2008; Riousset et al., 2010). The radiosonde (Figure S1) suggests that there was a strong wind shear above 7.5 km and the wind speed was increased rapidly from 13.7 to 17.02 km altitude with strong winds at the cloud tops (70 knots/36 ms^{-1}). The screening charge layers may then be more complex and may have intermixed with positive regions of the cloud. This condition would explain why two of fourteen discharges were found to correlate with positive polarity strokes of high peak currents (64,102 kA) (Table S1), rather than with negative strokes, as the 12 remainder discharges, expected for corona discharges and negative NBEs at cloud tops (Chou et al., 2018; F. Liu et al., 2018; Li et al., 2021).

We note here that 4 out of the 14 discharges appeared to generate elves, as also observed for another storm in Neubert et al. (2021). They are marked as "double" in table S1, and are associated with the highest currents detected by GLD360. Elves are most commonly generated by negative lightning strokes with high peak currents and fast rise-times (Barrington-Leigh & Inan, 1999; Rakov, 2003; Marshall, 2012), however here, two of the elves are from positive polarity currents. These are in our case streamer flash currents that should be able to generate elves weather oriented up- or downwards. This opens the question if not some of the elve events from positive strokes observed in the past are from blue corona discharges high in the clouds.

Data Availability Statement

Acknowledgments

References

Barrington-Leigh, C. P., & Inan, U. S. (1999). Elves triggered by positive and negative lightning discharges. *Geophysical Research Letters*, *26*(6), 683–686. doi: 10.1029/1999GL900059

Bessho, K., Date, K., Hayashi, M., Ikeda, A., Imai, T., Inoue, H., ... Yoshida, R. (2016). An Introduction to Himawari-8/9- Japan's New-Generation Geostationary Meteorological Satellites. *Journal of the Meteorological Society of Japan. Ser. II*, *94*(2), 151–183. Retrieved from https://www.jstage.jst.go.jp/article/jmsj/94/2/94_2016-009/_article doi: 10.2151/jmsj.2016-009

Boggs, L. D., Liu, N., Riousset, J. A., Shi, F., Lazarus, S., Splitt, M., & K. Rassoul, H. (2018). Thunderstorm charge structures producing gigantic jets. *Scientific Reports*, *8*(1), 1–12. doi: 10.1038/s41598-018-36309-z

Chanrion, O., Neubert, T., Lundgaard Rasmussen, I., Stoltze, C., Tcherniak, D., Jessen, N. C., ... Lorenzen, M. (2019). The Modular Multispectral Imaging Array (MMIA) of the ASIM Payload on the International Space Station. *Space Science Reviews*, *215*(4). Retrieved from http://dx.doi.org/10.1007/s11214-019-0593-y doi: 10.1007/s11214-019-0593-y

Chanrion, O., Neubert, T., Mogensen, A., Yair, Y., Stendel, M., Singh, R., & Siingh, D. (2017). Profuse activity of blue electrical discharges at the tops of thunderstorms. *Geophysical Research Letters*, *44*(1), 496–503. doi: 10.1002/2016GL071311

Chou, J. K., Hsu, R. R., Su, H. T., Chen, A. B. C., Kuo, C. L., Huang, S. M., ... Wu, Y. J. (2018). ISUAL-Observed Blue Luminous Events: The Associated Sferics. *Journal of Geophysical Research: Space Physics*, *123*(4), 3063–3077. doi: 10.1002/2017JA024793

Chou, J. K., Kuo, C. L., Tsai, L. Y., Chen, A. B., Su, H. T., Hsu, R. R., ... Lee, L. C. (2010). Gigantic jets with negative and positive polarity streamers. *Journal of Geophysical Research: Space Physics*, *115*(A7), 1–13. Retrieved from http://doi.wiley.com/10.1029/2009JA014831 doi: 10.1029/2009JA014831

Christian, H. J., Blakeslee, R. J., & Goodman, S. J. (1989). The detection of lightning from geostationary orbit. *Journal of Geophysical Research*, *94*(D11), 329–337. doi: 10.1029/jd094id11p13329

Edens, H. E. (2011). Photographic and lightning mapping observations of a blue starter over a New Mexico thunderstorm. *Geophysical Research Letters*, *38*(17), 1–4. doi: 10.1029/2011GL048543

Jacobson, A. R., & Heavner, M. J. (2005). Comparison of Narrow Bipolar Events with Ordinary Lightning as Proxies for Severe Convection. *Monthly Weather Review*, *135*(4), 1354–1363. doi: 10.1175/MWR3342.1

Karunarathna, N., Marshall, T. C., Stolzenburg, M., & Karunarathne, S. (2015). Narrow bipolar pulse location compared to thunderstorm radar echo structure. *Journal of Geophysical Research : Atmospheres*, *175*(4449), 238. doi: 10.1038/175238c0

Krehbiel, P. R., Riousset, J. A., Pasko, V. P., Thomas, R. J., Rison, W., Stanley, M. A., & Edens, H. E. (2008). Upward electrical discharges from thunderstorms. *Nature Geoscience*, *1*(4), 233–237. doi: 10.1038/ngeo162

Kuo, C. L., Chou, J. K., Tsai, L. Y., Chen, A. B., Su, H. T., Hsu, R. R., ... Lee, L. C. (2009). Discharge processes, electric field, and electron energy in ISUAL recorded gigantic jets. *Journal of Geophysical Research: Space Physics*, *114*(4), 1–10. doi: 10.1029/2008JA013791

Laroche, H. D. ·. S. U., Pierre · Betz. (2009). *Lightning: Principles, Instruments and Applications: Review of Modern Lightning Research*. Springer. doi: 10.1007/978-1-4020-9079-0{_}3

Lazarus, S. M., Splitt, M. E., Brownlee, J., Spiva, N., & Liu, N. (2015). A Thermodynamic, kinematic and microphysical analysis of a jet and gigantic jet-producing Florida thunderstorm. *Journal of Geophysical Research : Atmospheres*, *120*(May 2005), 8469–8490. doi: 10.1002/2015JD023383.Received

Li, D., Luque, A., Gordillo-Vázquez, F. J., Liu, F., Lu, G., Neubert, T., ... Reglero, V.

(2021). Blue Flashes as Counterparts to Narrow Bipolar Events: the Optical Signal of Shallow In-Cloud Discharges. *Journal of Geophysical Research: Atmospheres*, 1–13. doi: 10.1029/2021jd035013

Liu, F., Zhu, B., Lu, G., Lei, J., Shao, J., Chen, Y., ... Zhou, H. (2021). Meteorological and Electrical Conditions of Two Mid-latitude Thunderstorms Producing Blue Discharges. *Journal of Geophysical Research: Atmospheres*, *126*(8), 1–13. doi: 10.1029/2020jd033648

Liu, F., Zhu, B., Lu, G., Qin, Z., Lei, J., Peng, K. M., ... Zhou, H. (2018). Observations of Blue Discharges Associated With Negative Narrow Bipolar Events in Active Deep Convection. *Geophysical Research Letters*, *45*(6), 2842–2851. doi: 10.1002/2017GL076207

Liu, N., McHarg, M. G., & Stenbaek-Nielsen, H. C. (2015). High-altitude electrical discharges associated with thunderstorms and lightning. *Journal of Atmospheric and Solar-Terrestrial Physics*, *136*, 98–118. Retrieved from http://dx.doi.org/10.1016/j.jastp.2015.05.013 doi: 10.1016/j.jastp.2015.05.013

Lyons, W. A., Nelson, T. E., Armstrong, R. A., Pasko, V. P., & Stanley, M. A. (2003). Upward electrical discharges from thunderstorm tops. *Bulletin of the American Meteorological Society*, *84*(4), 445–454. doi: 10.1175/BAMS-84-4-445

Marchand, M., Hilburn, K., & Miller, S. D. (2019). Geostationary Lightning Mapper and Earth Networks Lightning Detection Over the Contiguous United States and Dependence on Flash Characteristics. *Journal of Geophysical Research: Atmospheres*, *124*(21), 11552–11567. doi: 10.1029/2019JD031039

Marshall, R. A. (2012). An improved model of the lightning electromagnetic field interaction with the D-region ionosphere. *Journal of Geophysical Research: Space Physics*, *117*(3), 1–15. doi: 10.1029/2011JA017408

Meyer, T. C., Lang, T. J., Rutledge, S. A., Lyons, W. A., Cummer, S. A., Lu, G., & Lindsey, D. T. (2013). Radar and lightning analyses of gigantic jet-producing storms. *Journal of Geophysical Research Atmospheres*, *118*(7), 2872–2888. doi: 10.1002/jgrd.50302

Neubert, T., Chanrion, O., Heumesser, M., Dimitriadou, K., Husbjerg, L., Rasmussen, I. L., ... Reglero, V. (2021). Observation of the onset of a blue jet into the stratosphere. *Nature*, *589*(7842), 371–375. Retrieved from http://dx.doi.org/10.1038/s41586-020-03122-6 doi: 10.1038/s41586-020-03122-6

Neubert, T., Østgaard, N., Reglero, V., Blanc, E., Chanrion, O., Oxborrow, C. A., ... Bhanderi, D. D. (2019). The ASIM Mission on the International Space Station. *Space Science Reviews*, *215*(2). Retrieved from http://dx.doi.org/10.1007/s11214-019-0592-z doi: 10.1007/s11214-019-0592-z

Rakov, V. A. (2003). Lightning electric field intensity at high altitudes: Inferences for production of elves. *Journal of Geophysical Research*, *108*(D20), 1–6. doi: 10.1029/2003jd003618

Riousset, J. A., Pasko, V. P., Krehbiel, P. R., Rison, W., & Stanley, M. A. (2010). Modeling of thundercloud screening charges: Implications for blue and gigantic jets. *Journal of Geophysical Research: Space Physics*, *115*(A1), n/a-n/a. doi: 10.1029/2009ja014286

Rison, W., Krehbiel, P. R., Stock, M. G., Edens, H. E., Shao, X. M., Thomas, R. J., ... Zhang, Y. (2016). Observations of narrow bipolar events reveal how lightning is initiated in thunderstorms. *Nature Communications*, *7*, 1–12. Retrieved from http://dx.doi.org/10.1038/ncomms10721 doi: 10.1038/ncomms10721

Said, R. K., Cohen, M. B., & Inan, U. S. (2013). Highly intense lightning over the oceans: Estimated peak currents from global GLD360 observations. *Journal of Geophysical Research Atmospheres*, *118*(13), 6905–6915. doi: 10.1002/jgrd.50508

Said, R. K., & Murphy, M. J. (2016). GLD360 Upgrade: Performance Analysis and Applications. *24th International Lightning Detection Conference*(Ic).

Soler, S., Pérez-Invernón, F. J., Gordillo-Vázquez, F. J., Luque, A., Li, D., Malagón-Romero, A., ... Østgaard, N. (2020). Blue Optical Observations of Narrow Bipolar Events by ASIM Suggest Corona Streamer Activity in Thunderstorms. *Journal of Geophysical Research: Atmospheres*, *125*(16). Retrieved from https://doi.org/10.1029/

2020JD032708 doi: 10.1029/2020JD032708

Stolzenburg, M., Rust, W. D., & Marshall, T. C. (1998). Electrical structure in thunderstorm convective regions 2. Isolated storms. *Journal of Geophysical Research Atmospheres*, *103*(D12), 14079–14096. doi: 10.1029/97JD03547

Suzuki, T., Hayakawa, M., Hobara, Y., & Kusunoki, K. (2012). First detection of summer blue jets and starters over Northern Kanto area of Japan: Lightning activity. *Journal of Geophysical Research: Space Physics*, *117*(7), 1–12. doi: 10.1029/2011JA017366

Tilles, J. N., Liu, N., Stanley, M. A., Krehbiel, P. R., Rison, W., Stock, M. G., ... Wilson, J. (2019). Fast negative breakdown in thunderstorms. *Nature Communications*, *10*(1), 1–12. Retrieved from http://dx.doi.org/10.1038/s41467-019-09621-z doi: 10.1038/s41467-019-09621-z

Van Der Velde, O. A., Bór, J., Li, J., Cummer, S. A., Arnone, E., Zanotti, F., ... Farges, T. (2010). Multi-instrumental observations of a positive gigantic jet produced by a winter thunderstorm in Europe. *Journal of Geophysical Research Atmospheres*, *115*(24), 1–17. doi: 10.1029/2010JD014442

van der Velde, O. A., Lyons, W. A., Nelson, T. E., Cummer, S. A., Li, J., & Bunnell, J. (2007). Analysis of the first gigantic jet recorded over continental North America. *Journal of Geophysical Research Atmospheres*, *112*(20), 2–10. doi: 10.1029/2007JD008575

Wescott, E. M., Sentman, D., Osborne, D., Hampton, D., & Heavner, M. (1995). Preliminary results from the Sprites94 Aircraft Campaign: 2. Blue jets. *Geophysical Research Letters*, *22*(10), 1209–1212. doi: 10.1029/95GL00582

Wiens, K. C., Hamlin, T., Harlin, J., & Suszcynsky, D. M. (2008). Relationships among Narrow Bipolar Events , " total " lightning , and radar-inferred convective strength in Great Plains thunderstorms. , *113*, 1–31. doi: 10.1029/2007JD009400

Wu, T., Dong, W., Zhang, Y., Funaki, T., Yoshida, S., Morimoto, T., ... Kawasaki, Z. (2012). Discharge height of lightning narrow bipolar events. , *117*(March), 1–13. doi: 10.1029/2011JD017054

Wu, T., Takayanagi, Y., Yoshida, S., Funaki, T., Ushio, T., & Kawasaki, Z. (2013). Spatial relationship between lightning narrow bipolar events and parent thunderstorms as revealed by phased array radar. *Geophysical Research Letters*, *40*(3), 618–623. doi: 10.1002/grl.50112

Zipser E.J. & Lutz K.R. (1994). The vertical profile of radar reflectivity of convective cells: A strong indicator of storm intensity and lightning probability? *Monthly Weather Review*, *122*, 1751–1759.
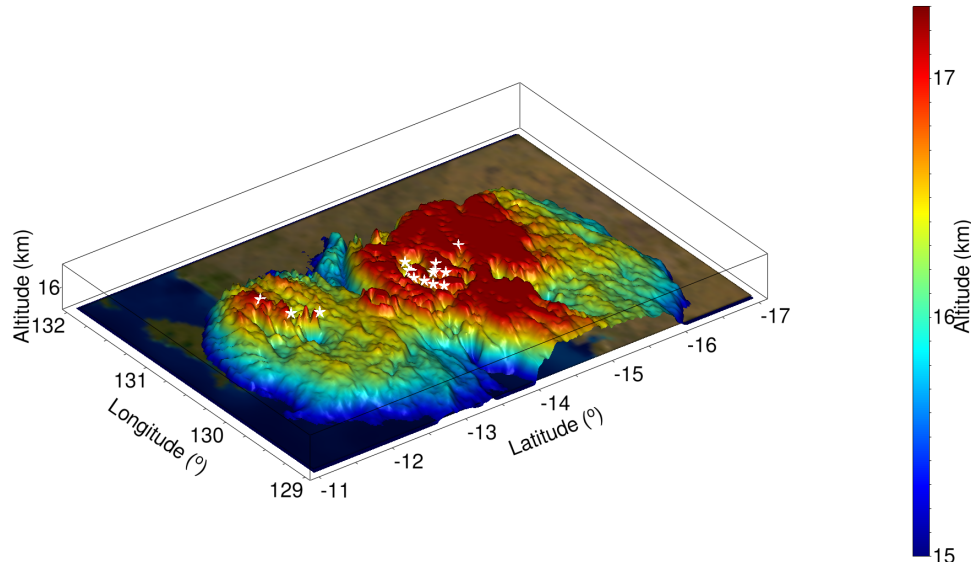
463

Figure 1. The cloud top altitude of the multi-cell thunderstorm over Northern Australia on 30 January 2021 at 17:00 UTC. The altitude is reconstructed by the Himawari satellite and the atmospheric sounding. The white starts indicate the position of the blue corona discharges, derived by the ASIM data.
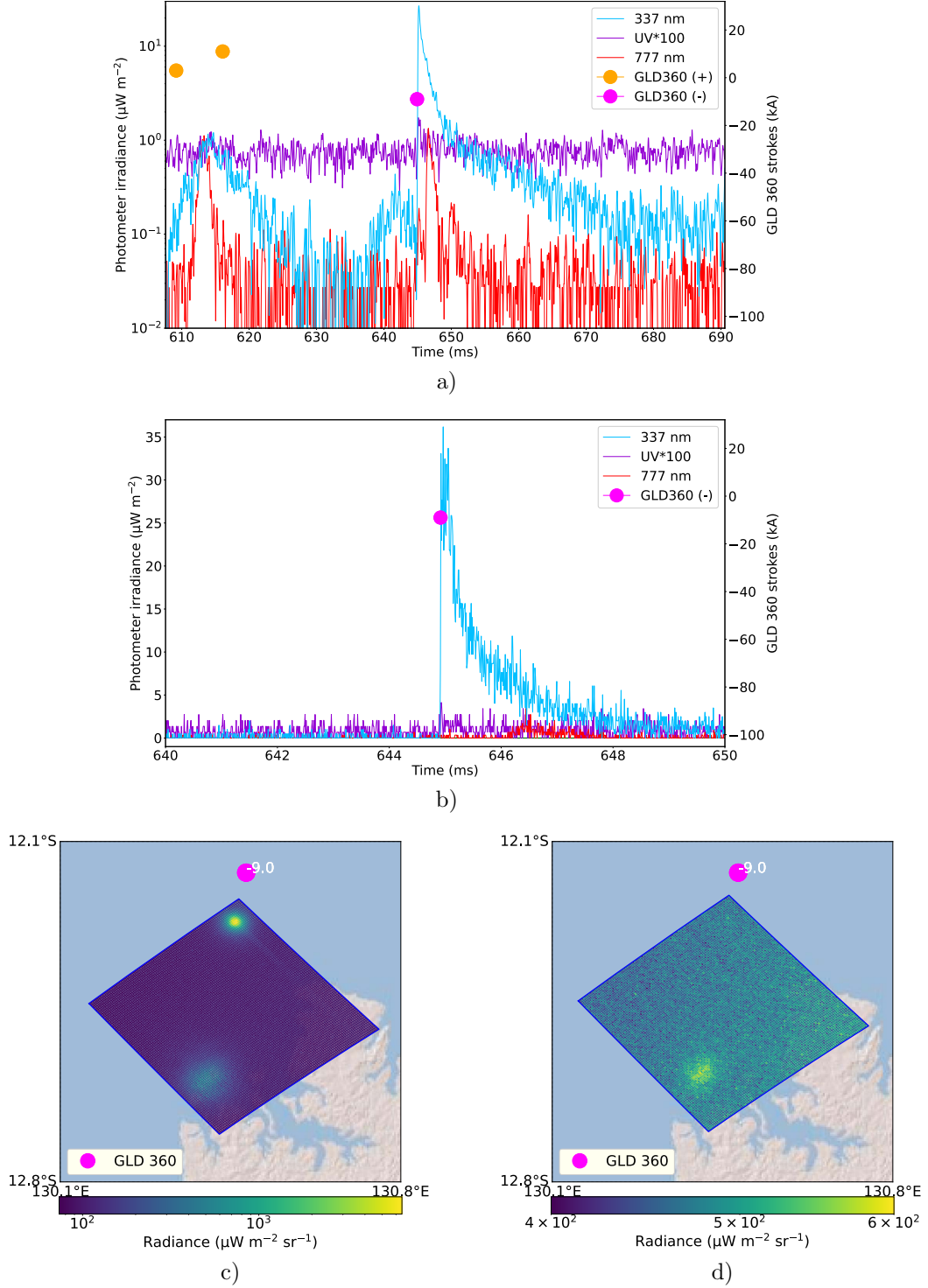
Figure 2. Blue corona discharge in a dissipating cell. a) Photometer signals corresponding to the blue pulse and accompanying UV and red signals, on logarithmic scale and 5-point Gaussian filtered. Concurrent GLD strokes (dots) displayed on top. t=0 corresponds to 30 January 2019 17:02:22.441 UTC. The time range of the photometer matches the exposure time of the respective camera frame (∼83.3 ms). b) Photometer signals around the blue corona discharge, on linear scale and non-filtered. c) 337.0 nm and d) 777.0 nm camera images projected on an altitude of 16 km. GLD strokes occurring within the integration time are displayed on top. The display images are the cropped and downloaded MMIA images with the observed activity.
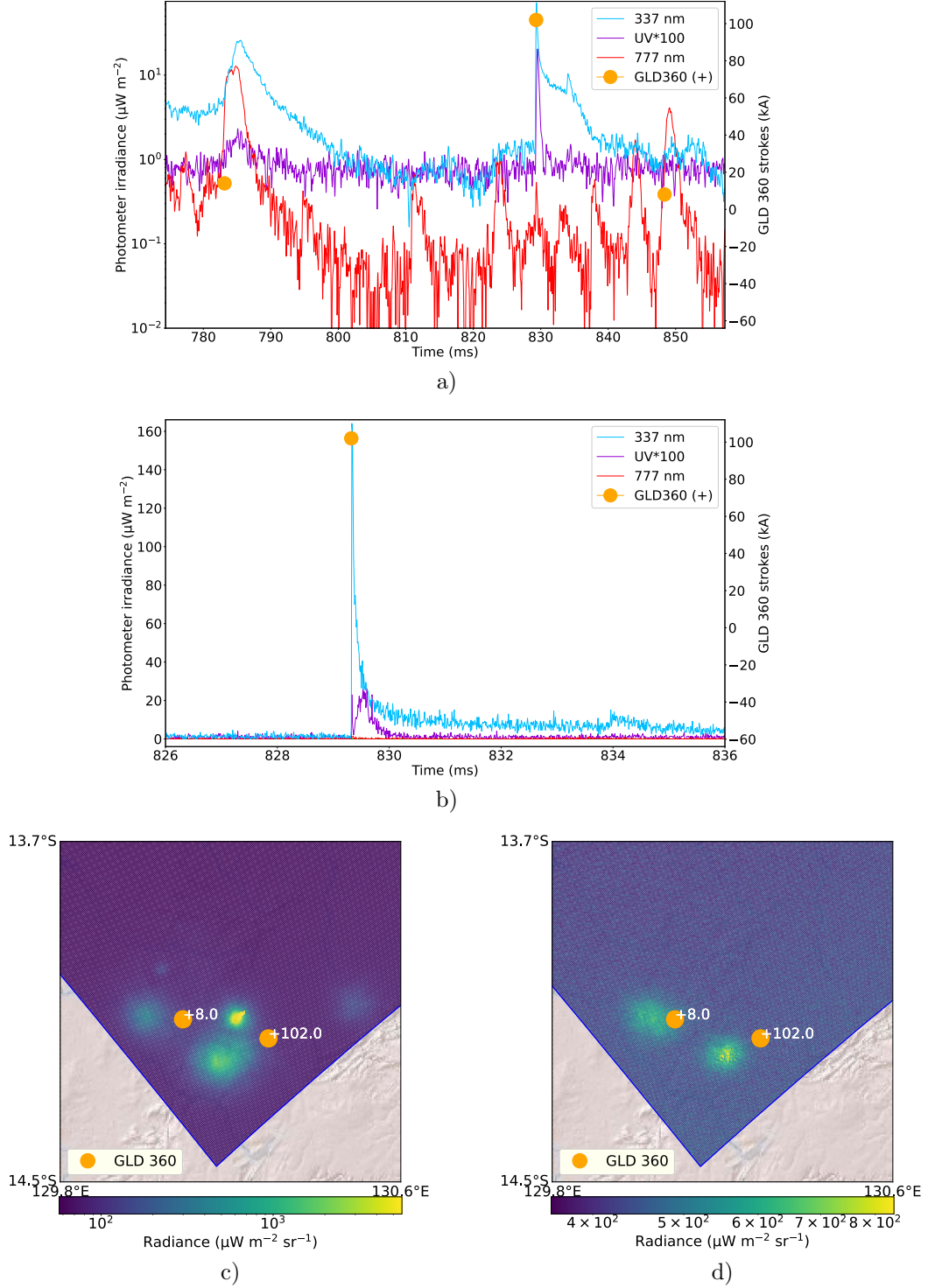
Figure 3. Blue corona discharge in a developing cell. a) Photometer signals corresponding to the blue pulse and accompanying UV and red signals, on logarithmic scale and 5-point Gaussian filtered. Concurrent GLD strokes (dots) displayed on top. t=0 corresponds to 30 January 2019 17:02:48.525 UTC. The time range of the photometer matches the exposure time of the respective camera frame (∼83.3 ms). b) Photometer signals around the blue corona discharge, on linear scale and non-filtered. c) 337.0 nm and d) 777.0 nm camera images projected on an altitude of 16 km. GLD strokes occurring within the integration time are displayed on top. The display images are the cropped and downloaded MMIA images with the observed activity.
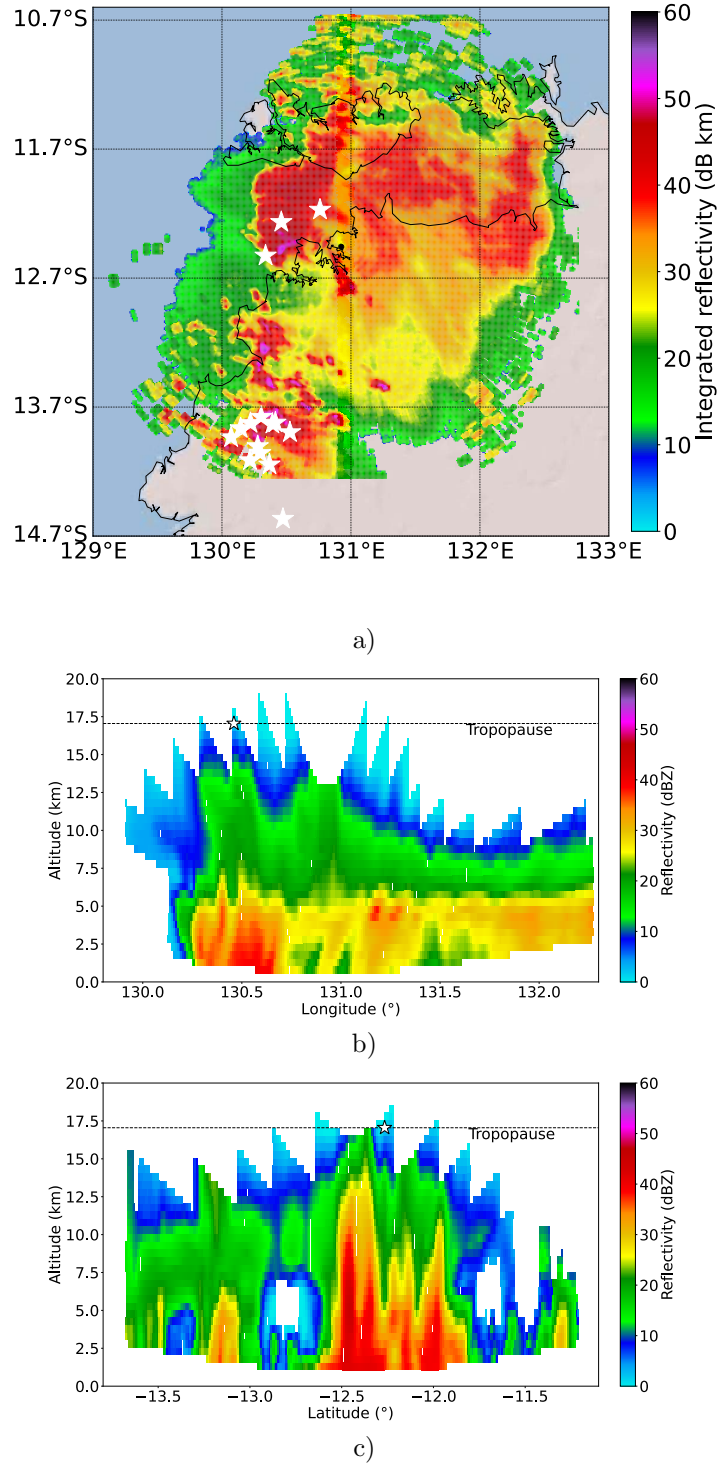
a)

b)

c)

Figure 4. a) The radar integrated reflectivity of the multi-cell thunderstorm over Northern Australia on 30 January 2021 at 17:00:31 UTC. The white starts indicate the position of the blue corona discharges. b) The vertical cross sections along -12.27° latitude. The white star indicates the longitude of the blue corona discharge. c) The vertical cross section along 130.47° longitude. The white star indicates the latitude of the blue corona discharge. The dashed line shows the altitude of the tropopause as derived by the sounding.

Supporting Information for "Analysis of blue corona discharges at the top of tropical thunderstorm clouds in different phases of convection"

Krystallia Dimitriadou[1], Olivier Chanrion[1], Torsten Neubert[1], Alain Protat[2],

Valentin Louf[2], Matthias Heumesser[1], Lasse Husbjerg[1], Christoph Köhn[1],

Nikolai Østgaard[3], and Victor Reglero[4]

[1]National Space Institute, Technical University of Denmark (DTU Space), Kgs. Lyngby, Denmark

[2]Australian Bureau of Meteorology, Science and Innovation Group, Radar Science and Nowcasting Team, Melbourne, Australia

[3]University of Bergen, Birkeland Centre for Space Science, Bergen, Norway

[4]University of Valencia, Image Processing Laboratory, Valencia, Spain

Contents of this file

―――――

Corresponding author: K. Dimitriadou, DTU Space, Technical University of Denmark, Elektrovej, Building 327, 2800 Kgs. Lyngby, Denmark. (krstd@space.dtu.dk)

August 24, 2021, 1:25pm

Introduction This supplementary information contains plots adding more details to the observations described in the main manuscript. The calculation of the rise times of the blue corona discharges is described thoroughly. For the blue corona discharges accompanied by an elve, we expain in detail what a single and what a double UV pulse mean. Furthermore, we provide information about the atmospheric sounding that characterized the thunderstorm environment where blue corona discharges were facilitated from. Last, we describe all the possible errors induced by projection offsets, different spatial resolutions of the instruments/detectors involved.

1. Rise time calculation

In order to calculate the rise times of the BEDs we implemented an algorithm which processes the whole sequence of ASIM observations in the storm and work as follows:

1. [Find all blue peaks]. It finds all the peaks in the blue photometer that increase by more than 5 $\mu W/m^2$ in 5 samples. The rise time is calculated by counting the number of samples it takes for the BED event to increase from 10% of the full amplitude to 90% of the full amplitude

2. [Disregard peaks close to each other] If several peaks occur within 500 samples, it disregards all except the biggest peak.

3. [Disregard delta peaks (cosmic rays)] It sums the blue photometer data together, 100 samples before and after the peak, and take the ratio as (after)/(before). If this ratio is below 2.97, it disregards the blue peak. Note that a lower ratio here suggests highly narrow peaks like cosmic rays.

4. [Disregard peaks where the red photometer is large] It sums blue and red photometer data up 50 samples before the peak and 150 samples after the peak and take their ratio, i.e. sum(phot3[i-50:i+150])/sum(phot1[i-50:i+150]) where i is the peak index. If this ratio is below 0.15 it considers the peak a BED.

In general, the step 1 results in hundreds of peaks, which then are reduced to tens of peaks in step 2, down to single or no peaks in step 3 and 4. All the values in the algorithm are found empirically.

2.   Single and double UV signals

10 out of the 14 blue pulses are associated with a UV signal in the 180-230 nm (VUV) ASIM photometer. Those signals are characterised as either single or double pulses depending on how many peaks are identified. 4 out of 10 of UV signals are double, indicating that the VUV photometer has recorded signals from both the blue discharge and the accompanying elve. In the remaining 6 signals, characterized as single pulses, the VUV photometer records only the signal from the blue discharges emanating from the cloud top.

3.   The atmospheric sounding

Figure S1 displays a Skew-T log-P diagram, commonly known as an atmospheric/ balloon sounding or radiosonde. Such diagrams are important both for weather forecasting models and assessing the atmospheric conditions in a give time and place. They provide information regarding the stability or instability of the atmosphere, pinpoint weather elements (temperature, dew point, wind speed and direction etc.) in all layers of the atmosphere as well as important atmospheric indices (CAPE, CIN, K index etc.), important for the categorization of convection environments.

The basic lines that constitute such diagram are the isobars on the vertical axis, solid lines of equal pressure that run horizontally and with the space between the pressure levels to change, thus the log-P. Pressure is mostly given every 100 hPa but the presented sounding indicates more levels in between. In each pressure level the corresponding altitude is give next to it in metres. Pressure height is preferred instead of the actual typical height, since pressure is not constant in the upper atmosphere (low and high pressure

systems). On the horizontal axis, there are the valus of the isotherms, solid lines of equal temperature than run vertically. There are three additional types of lines, the saturation mixing ratio lines, the dry adiabatic lapse rates line and the moist adiabatic lapse rate lines which are out of the scope of this study, therefore will not be discusses. Last, on the right of the diagram, the wind barbs are plotted which indicate the wind speed and direction for a given atmospheric layer. A wind bar points to the direction from which the winds are coming. The lines and triangle perpendicular to the wind bars indicate the speed of the wind. Half line is 5 knots, a full line is 10 knots and the triangle is 50 knots. Wind speed is calculated from the summation of all the lines and triangles.

In the diagram, two intense and one faint black lines are plotted. From left to the right, the first line is the dewpoint plot. Dewpoint is related to the quantity of moisture in the air. The second line is the temperature measured in the atmosphere (or environmental sounding) and it is always to the right of the dew point line. The faint black curved line is the parcel lapse rate and indicates the path an air parcel will take if raised from the Planetary Boundary Layer (100 m - 2 km). This line is used for the calculation of thermodynamic indices such us CAPE (Convection Available Potential Energy), CIN (Convective INhibition), LI (Lifted Index) etc. CAPE, an index commonly used for characterising convection in storms, is the integration of positive area on a sounding. Positive area is defined the region where the the parcel temperature (curved thin black line) is warmer than the actual temperature (second line from the left). Depending on how close are the dewpoint and the temperature line we extract information about the

humidity and the saturation of air. In the presented sounding of Figure S1, the two lines are really close indicating a highly humid and saturated atmosphere in the given station.

4. Data uncertainties and induced errors

In Figure 1 of the manuscript, for displaying purposes, blue corona discharges are projected in 17 km altitude instead of the 16 km projection altitude in the ASIM cameras. This does not affect the physical meaning of the presented cases and is only preferred in order for the events to be clearly visible in the 3D plot. ASIM geolocation errors in the ground are up to 10 km. This might slightly affect the position of the blue events, as indicated on the cloud top altitudes (Figure 1) and on the radar data (Figure 4). The induced uncertainties in the position are not significant for the physical meaning of the data. Furthermore, one can note that the values of Cloud Top Temperature (CTT) and Cloud Top Height (CTH) refer to a spatial resolution of 2 km, which is the resolution of Himawari satellite.

In Figure 4b and c, the step feature (light blue peaks) is a result of the gridding technique of the radar data. When there is a gap between those areas, there are no observations from the discrete elevations the radar uses to sample the atmosphere and it is not certain if there is a cloud as high as either sides of those gaps.
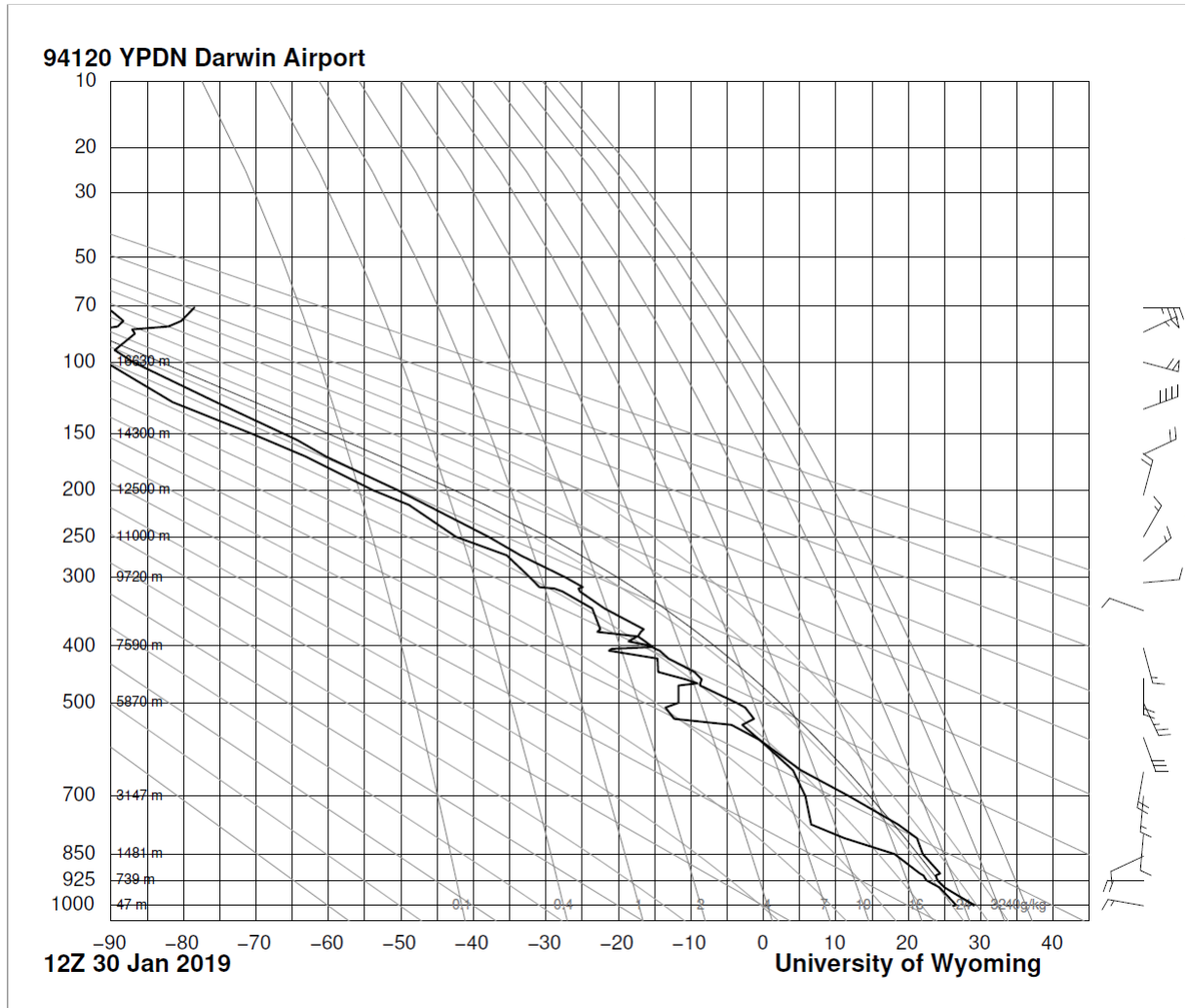
94120 YPDN Darwin Airport

Figure S1. Atmospheric Sounding (SkewT-logP) from Darwin Aiport at 12 UTC on January 30, 2019.
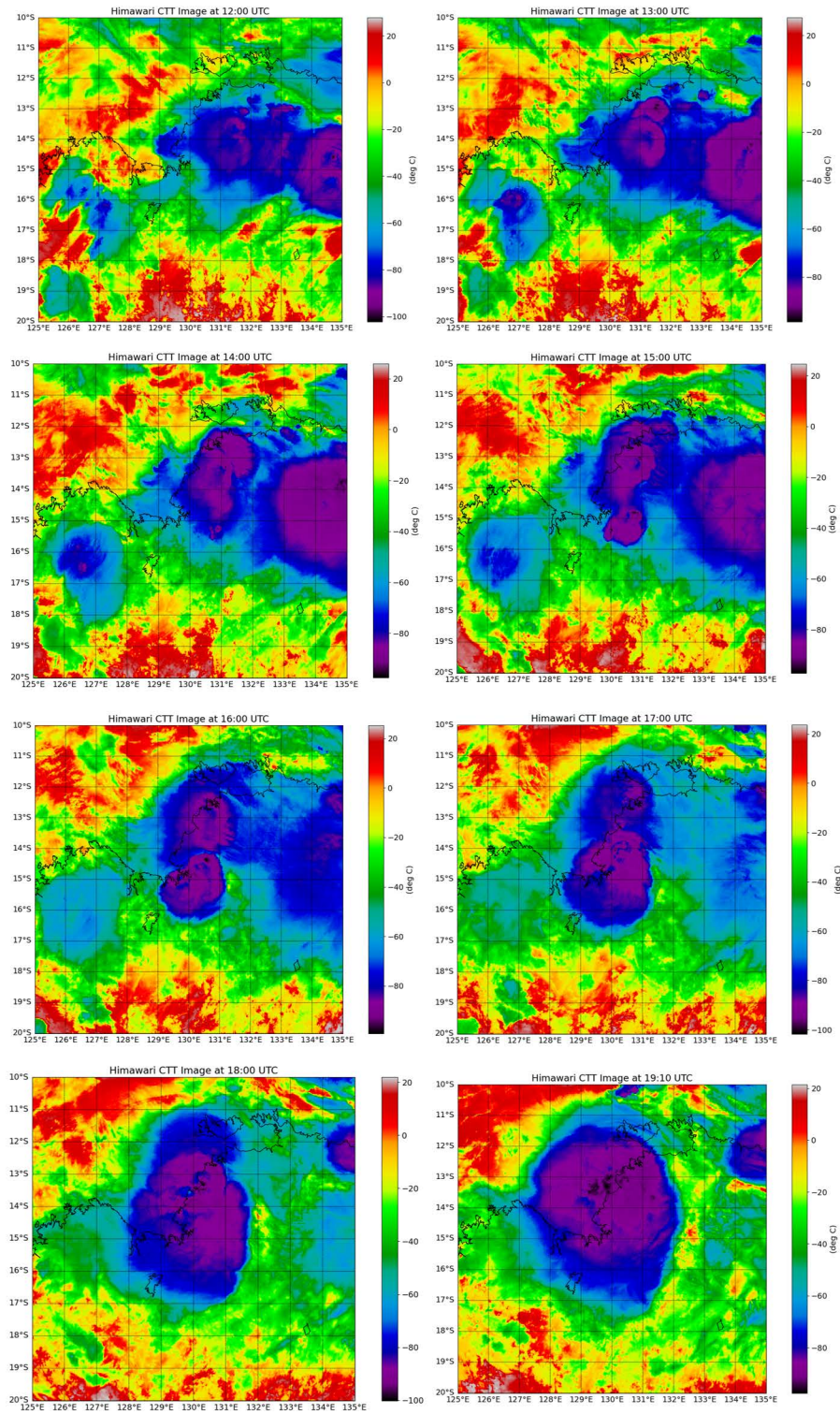
August 24, 2021, 1:25pm

Figure S2. Storm evolution every 1 hour, from 12 UTC to 19 UTC detected by the 10.4 IR channel (Brightness Temperature) of Himawari geostationary satellite.
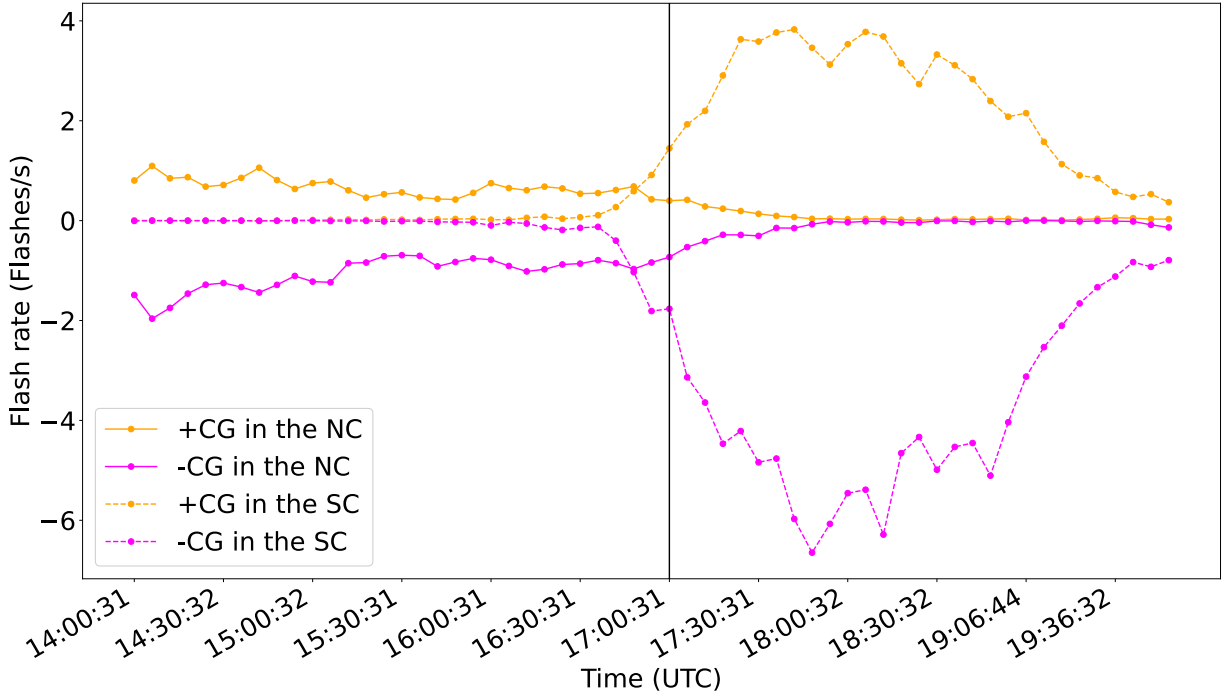
Figure S3. Flash rates of positive (orange) and negative (magenta) CGs in northern (straight line) and southern (dashed line) cells. The negative y-axis refer to the flash rates of all the negative strokes. Each point represents a radar scanning cycle (6 min) and the calculated flash rate is the average flash rate per cycle.
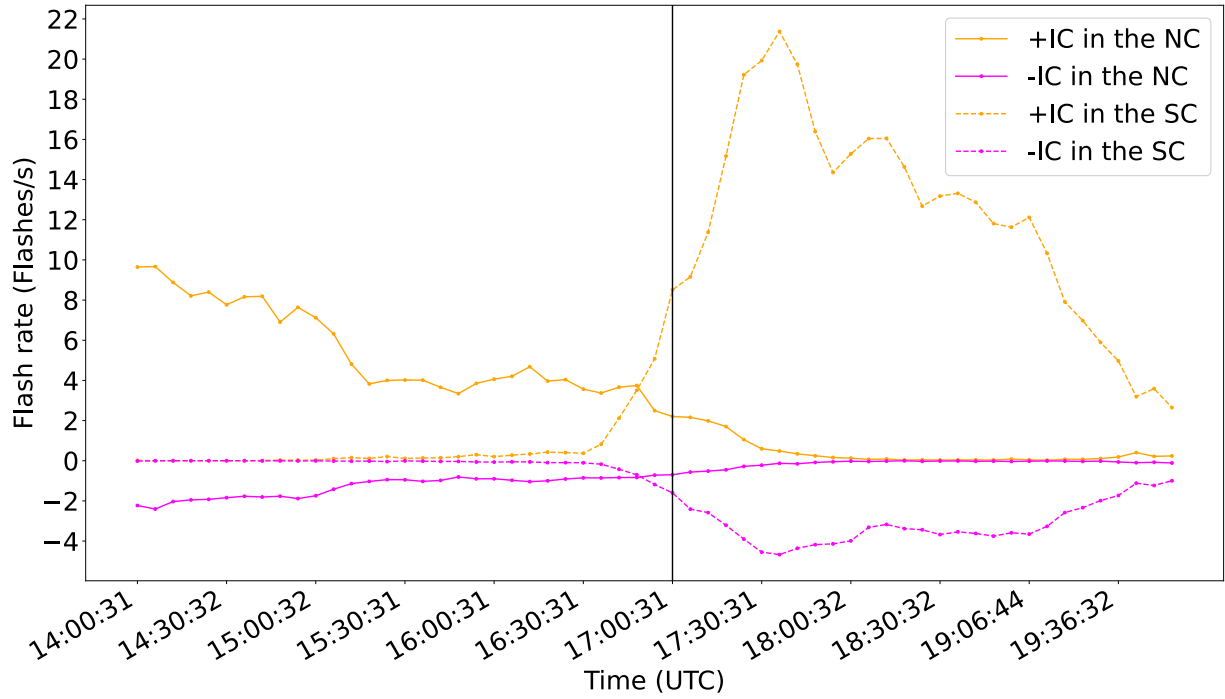
August 24, 2021, 1:25pm

Figure S4. Flash rates of positive (orange) and negative (magenta) ICs in northern (straight line) and southern (dashed line) cells. The negative y-axis refer to the flash rates of all the negative strokes. Each point represents a radar scanning cycle (6 min) and the calculated flash rate is the average flash rate per cycle.

Table S1.   Blue corona discharge electrical and meteorological properties

Blue flash time[a] (UTC)	Blue flash rise time (μs)	Accomp. UV pulse	UV pulse rise time (μs)	GLD or EN current (kA)	CG or IC[e]	Group of cells	CTT (°C)	CTH ($\pm$ 0.5) (km)	Reflectivity (dBZ km)
17:02:22.645	20	-	-	-9	IC	NC	-87	16.6	40
17:02:32.397	10	single	10-20	-50	CG	SC	-81	15.9	36
17:02:34.731	20	-	-	-9	IC	NC	-84	16.3	25
17:02:47.708	20	single	20-30	-54	CG	SC	-90	17+	43
17:02:48.829[b]	10	double	20-30 100	102	CG	SC	-88	16.7	38
17:02:50.855[c]	20	single	20-30	-32	CG	NC	-89	17	38
						SC	-83	16.2	49
17:02:54.327	10	-	-	-12	IC	SC	-90	17+	-
17:02:59.141	20	single	10	-144[d]	CG	SC	-91	17+	46
17:03:01.899[b]	20	double	10-20 100	64	CG	SC	-86	16.5	30
17:03:04.016	10	-	-	-19	CG	SC	-85	16.4	49
17:03:20.002[b]	20	double	20-30 60-70	-75	CG	SC	-88	16.8	34
17:03:21.392[b]	20	double	30 80	-79	CG	SC	-86	16.5	50
17:03:26.741	20	single	10-20	-54	CG	SC	-84	16.3	28
17:03:34.235	20	single	30-40	-72	CG	SC	-89	16.9	42

Abbreviations: NC=Northern group of cells, SC=Southern group of cells, CTT= Cloud Top Temperature, CTH=Cloud Top Height
[a]The time refers to the filtered photometer pulses.
[b]Blue flashes accompanied by double UV signals.
[c]Blue flash referring to two spots of activity within the same ASIM frame.
[d]Only observation with current reported by Earth Networks.
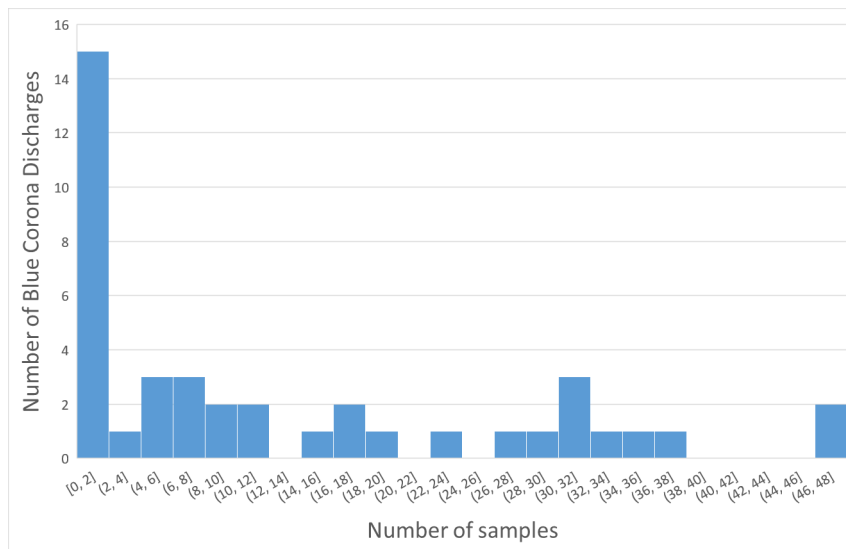[e] Classification provided by GLD and Earth Networks.

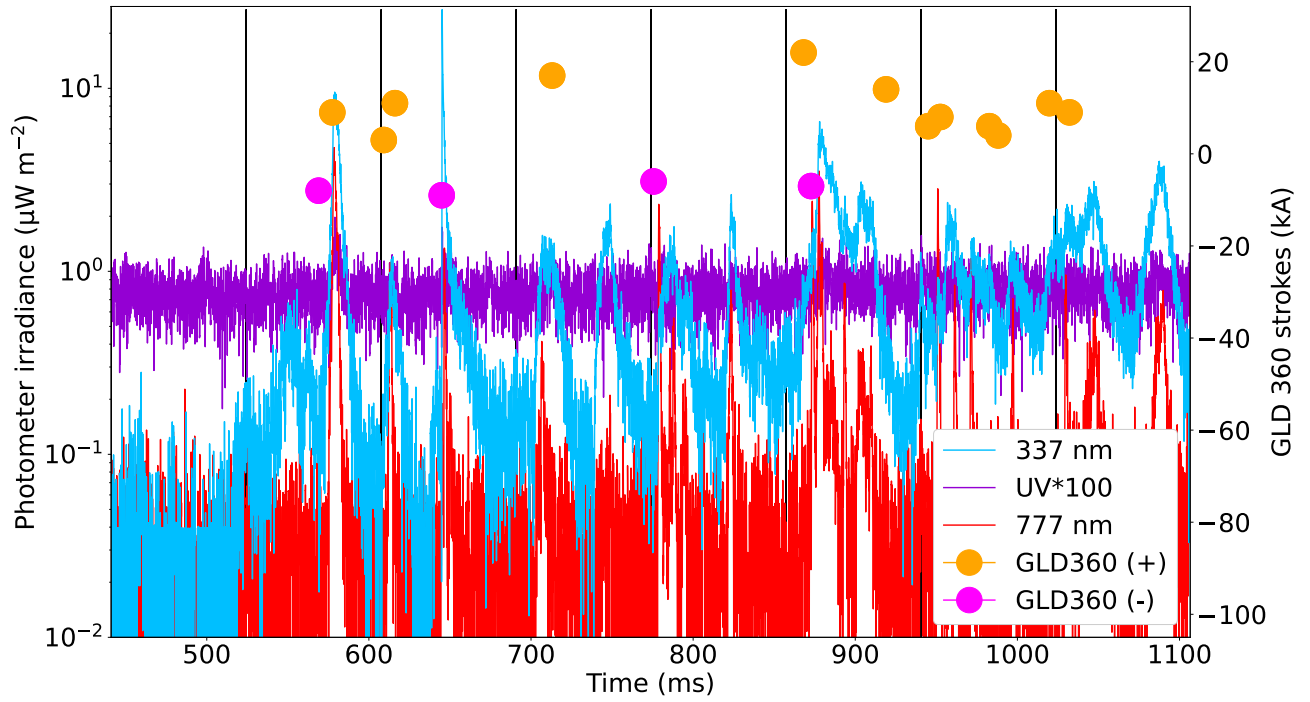**Figure S5.** Rise time distribution of Blue Corona Discharge emissions for the whole storm.

Figure S6. Blue Corona Discharge in a dissipating cell: Photometer signals of the whole MMIA event and GLD360 detections. Vertical lines mark the camera image exposure periods (∼83.3 ms). The frame of interest is Frame 3.
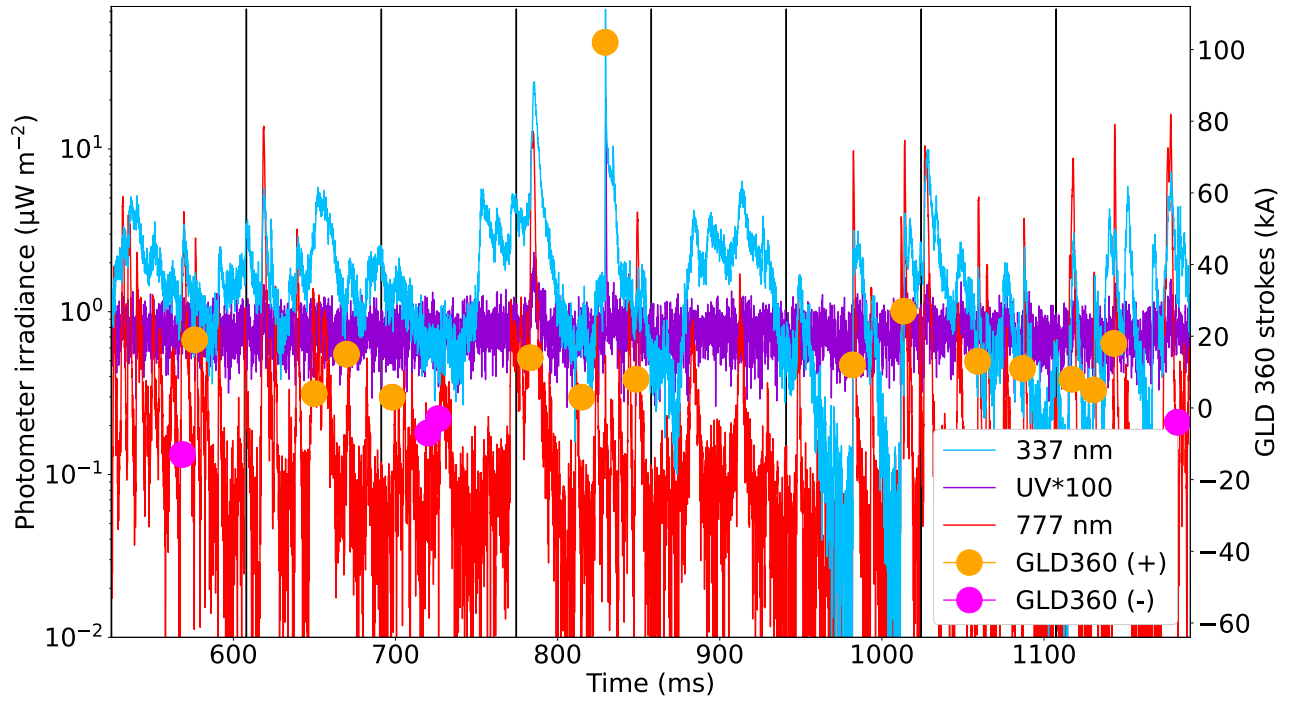
Figure S7.   Blue Corona Discharges in a developing cell: Photometer signals of the whole MMIA event and GLD360 detections. Vertical lines mark the camera image exposure periods(∼83.3 ms). The frame of interest is Frame 4.
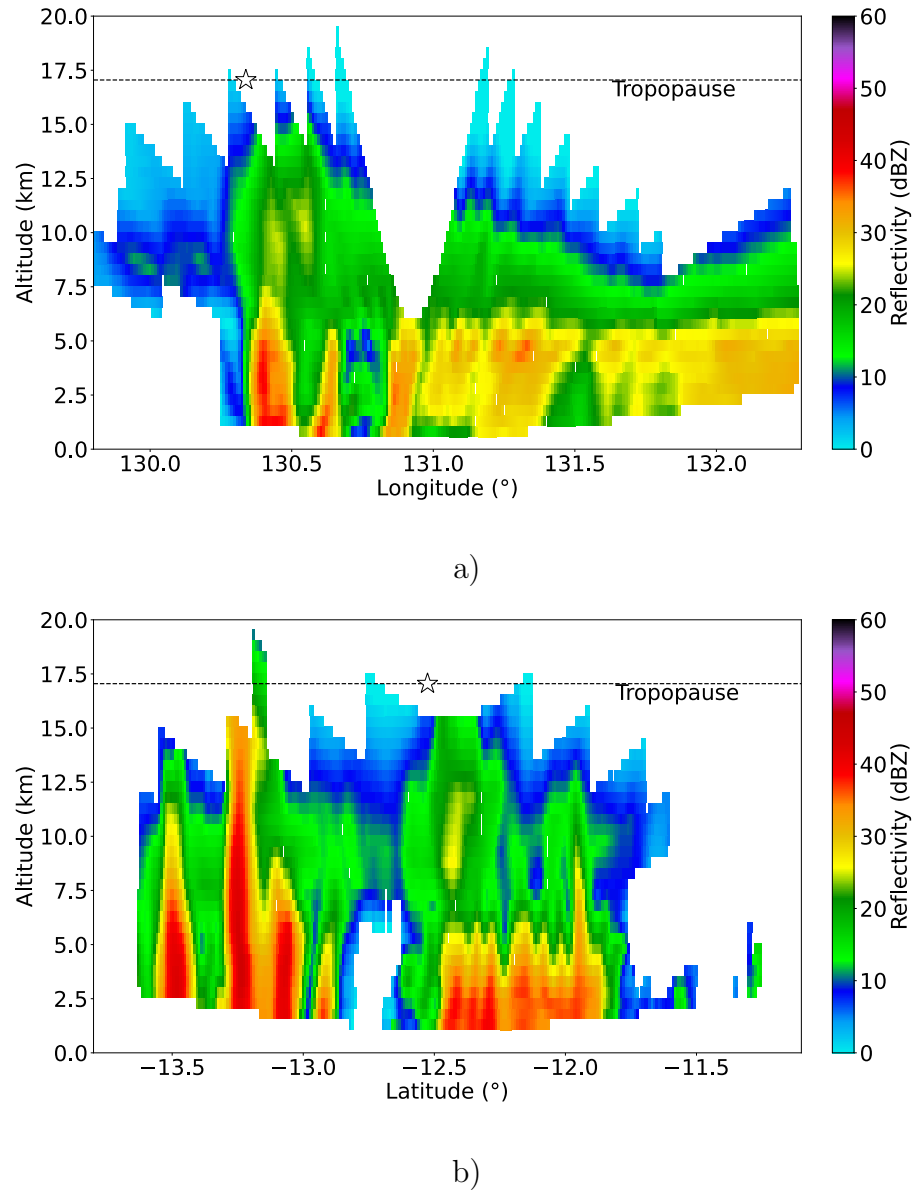
a)

b)

Figure S8. Additional cross sections in the Blue Corona Discharges of dissipating clouds: a) The vertical cross section along -12.53° latitude (BED latitude indicated by a '*'). b) The vertical cross section along 130.34° longitude (BED longitude indicated by a '*')
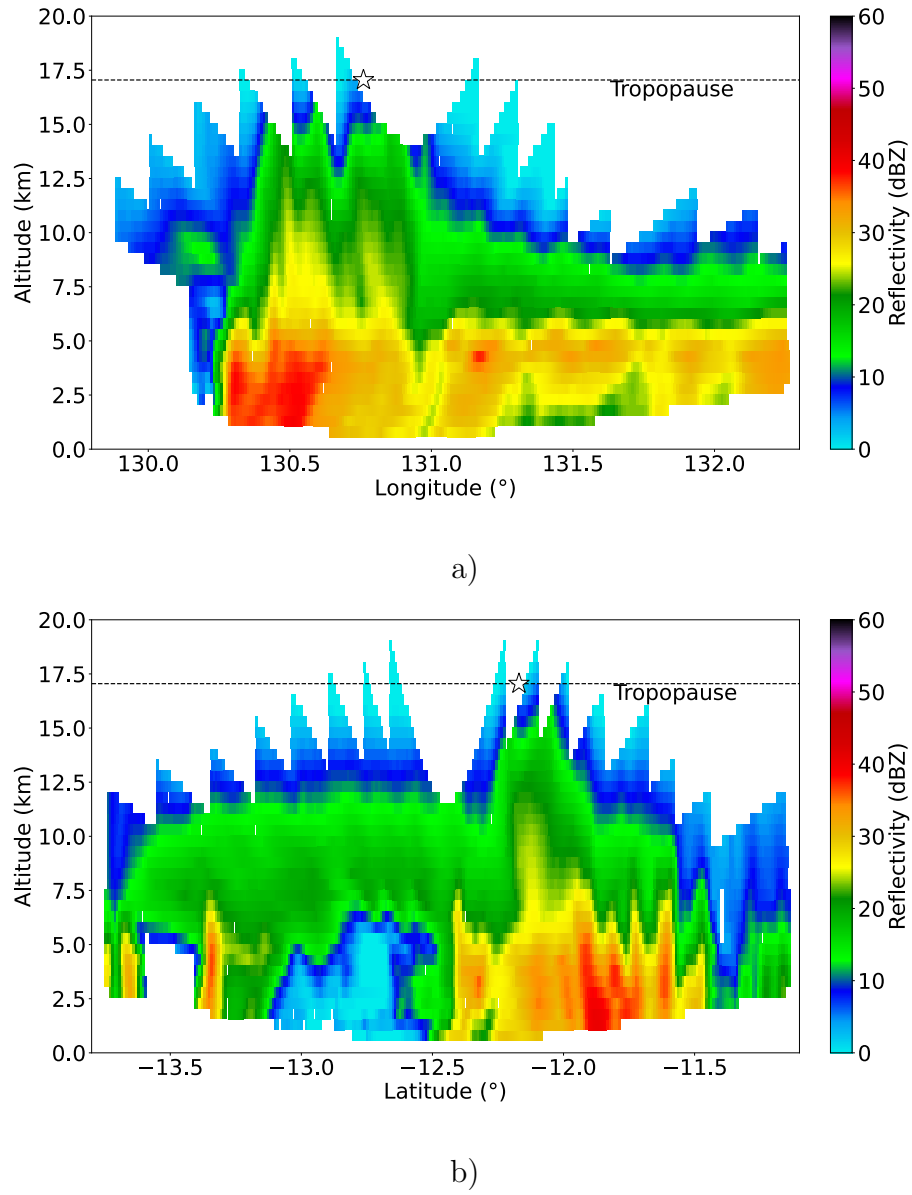
August 24, 2021, 1:25pm

a)

b)

Figure S9. Additional cross sections in the Blue Corona Discharges of dissipating clouds a) The vertical cross section along -12.17° latitude (BED latitude indicated by a '*'). b) The vertical cross section along 130.76° longitude (BED longitude indicated by '*')

August 24, 2021, 1:25pm